Density Functional Characterization of [$HClO_2$] Potential Energy Surface

Raman Sumathi and S. D. Peyerimhoff*

Lehrstuhl fur Theoretische Chemie, Universitat Bonn, Wegelerstrasse 12, D-53115 Bonn, Germany

Received: April 28, 1999; In Final Form: July 12, 1999

The potential energy surface (PES) of [$HClO_2$] system has been investigated at second-order Moller−Plesset perturbation (MP2) and density functional theory levels using, respectively, the 6-311++G** and 6-311++G-(2df,2pd) basis sets. The structural parameters of the isomers of [$HClO_2$] were also optimized at complete active space [(CAS(12,12)] self-consistent field level using the 6-31G** basis set. Three isomers of relative thermodynamic stability, HOOCl (**1**) > HOClO (**2**) > $HClO_2$ (**3**), have been identified as energy minima. Besides these covalently bound minima, various loose hydrogen-bonded complexes (OOH···Cl **5a(s)**, **5′a(t)**, and O···HOCl **7a(t)**) have been located on the singlet and triplet PES. Isomerization, molecular elimination, and direct hydrogen abstraction saddle points have been traced and a qualitative understanding of the mechanism and kinetics of the stratospherically important HO + ClO and HO_2 + Cl reactions has been derived.

Introduction

Stratospheric ozone abundance is largely determined by the rates of the catalytic chain processes which destroy ozone and by the concentration of the chain carriers and their precursors. Among various species, the radical carriers of the HO_x ($x = 1$, 2), ClO_x ($x = 0$, 1), BrO_x ($x = 0$, 1), and NO_x ($x = 1$, 2, 3) families have been identified as the major species in determining the ozone concentration in the Earth's atmosphere. Besides the concentration of these species, the rate coefficients of the reactions between these families are crucial as their interaction could lead to either another chain carrier (chain transfer) or a reservoir molecule. Our interest in recent years is to obtain meaningful potential energy surfaces (PES) for the reactions between these families (viz., HO_2 + NO,[1] HO + NO,[2] HO + NO_2,[1] H + NO_2,[2] etc.,) and to perform a detailed kinetic analysis using statistical methods. The results of such an analysis, the magnitude of the rate constant as well as their temperature, and pressure dependences could be used effectively in the studies of atmospheric modeling.

In this work, we investigate the radical−radical reaction between OH and ClO which potentially possesses two possibilities:

$$OH + ClO \xrightarrow{k_{1a}} HO_2 + Cl \qquad (1a)$$

$$OH + ClO \xrightarrow{k_{1b}} HCl + O_2 \qquad (1b)$$

viz., transfer of the chain carriers (reaction 1a) and formation of the reservoir molecule (reaction 1b). Consequently, the contribution of channel 1b to the total rate constant would clearly establish the importance of OH + ClO reaction in atmospheric chemistry.

There have been few previous studies on the kinetics of this reaction. Leu and Lin,[3] using the discharge flow−resonance fluorescence technique, measured the rate coefficient, k_1, at 298 K (9.1×10^{-12} cm^3 molecule^{-1} s^{-1}) and provided an upper limit on the branching ratio (k_{1a}/k_1) of 0.65. Ravishankara et al.[4] found that the reaction within experimental uncertainty is independent of temperature over the range 248−335 K and they reported a value of 1.7×10^{-11} cm^3 molecule^{-1} s^{-1} for k_1. Hill and Howard[5] using discharge flow−laser magnetic resonance technique, measured the rate constant at low pressures (1.0−1.1 Torr) and at temperatures between 219 and 373 K. They reported a negative temperature dependence for k_1 with a magnitude of k_1 equivalent to $(8.0 \pm 1.4) \times 10^{-12}$ exp[$(235 \pm 46)/T$] cm^3 molecule^{-1} s^{-1} and $k_{1a}/k_1 = 0.86 \pm 0.14$. Burrows et al.[6] independently reported a branching ratio of 0.85 ± 0.15 in agreement with Hill and Howard's work. However, they observed the reaction to be temperature independent with a relatively low magnitude for k_1 (50% lower) compared to ref 5. Poulet et al.,[7] using laser-induced fluorescence technique, derived a conclusion very similar to that of Hill and Howard.[5] Though all these investigations have consistently revealed the inconsequential role of channel 1b, the mechanism of the title reaction as to whether it involves any stable intermediates (temperature dependence) is not yet known clearly.

More importantly, several experiments[8−14] have been conducted to study the kinetics of the reaction products of (1a) viz.

$$HO_2 + Cl \rightarrow HCl + O_2 \qquad (2a)$$

$$HO_2 + Cl \rightarrow HO + ClO \qquad (2b)$$

The reported values of k_2 ranges from $2.1(-1.8) \times 10^{-11}$ to $(7.3 \pm 2.5) \times 10^{-11}$ cm^3 molecule^{-1} s^{-1}. The direct measurement of the rate constant and the branching ratio for reaction 2 by Lee and Howard[14] has led to a value of $(4.2 \pm 0.7) \times 10^{-11}$ cm^3 molecule^{-1} s^{-1} and 0.20 for k_2 and k_{2b}/k_2, respectively. Weissman et al.[15] performed a theoretical analysis on this reaction using the thermochemical parameters to explain the large magnitude of the rate constant observed in this and other radical−radical reactions. They reasoned that these large rate constants could not arise from the complex Cl···HO_2, leading to direct hydrogen abstraction products. Rather they suggested that the strongly attractive nature of the PES for chlorine attack on the terminal oxygen of HO_2 could lead to (HO_2···Cl] complex and thereby to a large collision cross section. They

* Corresponding author. Fax: 49-228-739064. E-mail: unt000@IBM.rhrz.uni-bonn.de.

10.1021/jp991390i CCC: $18.00
Published on Web 08/31/1999

invoked a four-center elimination from the HOOCl intermediate to yield HCl + O_2 and estimated an unusually low energy barrier for this path. Lee and Howard,[14] however, believed that the rate constant measured by them were within the estimated upper limits for direct hydrogen abstraction. Mozurkewich[16] performed a kinetic analysis based on thermochemically estimated vibrational frequencies and barrier heights and showed that the direct hydrogen abstraction is likely to predominate over HOOCl intermediate formation. Since there are no experimental studies that have isolated the HOOCl intermediate, the only pragmatic approach to clarify this point is to perform detailed ab initio calculations on the [$HClO_2$] surface and to identify the important stationary points associated with these mechanisms. Toohey and Anderson[17] studied the simple direct hydrogen abstraction process at the UMP2/6-31G** level of theory and estimated an activation barrier of 8.4 kcal/mol for this process. Though the other two existing theoretical works[18,19] on [$HClO_2$] system were done at a high level of ab initio investigation viz., CCSD-(T)/ANO4//CCSD(T)/TZ2P, they have concentrated only on the relative stability of the various isomers of [$HClO_2$] and of their stability relative to dissociation in addition to the predictions regarding the heat of formation and harmonic vibrational frequencies of [$HClO_2$] isomers. Therefore, as a first necessary step toward an understanding of the reaction kinetics of [$HClO_2$] isomers, we wish to establish its PES as complete as possible. In this regard, we consider here the possible isomerization, decomposition, dissociation, and direct hydrogen abstraction channels on the lowest lying singlet electronic surface. Since the ground electronic state of oxygen atom and oxygen molecule are respectively ^3P and $^3\Sigma_g^-$, the direct hydrogen abstraction channels leading to either atomic or molecular oxygen are also studied on their lowest triplet surface.

Since most of the dissociation channels, viz., HOOCl → HO + ClO, HOOCl → H + OOCl, HOOCl → Cl + HO_2, HOClO → H$^\bullet$ + OClO$^\bullet$, HOClO → HO$^\bullet$ + ClO$^\bullet$, are direct dissociations involving no specific saddle points, we need to treat these channels via variational or microvariational transition state theory in our kinetic analysis. This, in turn, demands for the complete PES of all these channels as a function of the dissociation bond lengths (R) and to obtain the harmonic vibrational frequencies of the partially optimized structures as a function of the possible R. Hence, for practical purposes it is essential to adopt the computationally less demanding and however meaningful density functional approach. In order to test the applicability of DFT to the system under investigation, we have optimized and compared the equilibrium geometries of the [$HClO_2$] isomers at B3LYP, second-order Moller−Plesset perturbation theory including all electrons for correlation (MP2-(fu)) as well as complete active space self-consistent field (CAS-(12,12)) levels. Furthermore, the hybrid B3LYP method has also been found[20] to yield realistic results for the prediction of the transition states' geometries and energies. In the HONO system, the B3LYP/6-311G(3df,3pd) predicted that barrier heights differ by less than 1 kcal/mol from those of the CBSQ computed values.[21] Nevertheless, our primary aim in this investigation is to identify the key intermediates and the reaction pathways and thereby to gain insight into the reaction kinetics.

Computational Details

All calculations were performed using the Gaussian 94 program.[22] Geometries of reactants, adducts, and transition state structures were optimized using the density functional approach with the popular hybrid B3LYP functional[23] in conjunction with analytical gradient methods. The exchange functional in the hybrid B3LYP method is composed of three terms, including the Hartree−Fock exchange functional. The correlation functional is that of Lee, Yang, and Parr.[24] The open-shell calculations were performed using the unrestricted formalism (UHF, UB3LYP). The potential energy surface was initially mapped out with B3LYP/6-31G** calculations. The identity of each first-order stationary point is determined when necessary by intrinsic reaction coordinate (IRC) calculations.[25] Geometries were then reoptimized with a larger, 6-311++G(2df,2pd) basis set. The zero-point energies were derived from harmonic vibrational wavenumbers at the (U)B3LYP/6-311++G(2df,2pd) level. MOLPRO[26] was employed to perform CAS calculations. Throughout this paper, bond lengths are given in angstroms, bond angles in degrees, zero-point and relative energies (obtained from DFT) in kcal/mol, unless otherwise stated.

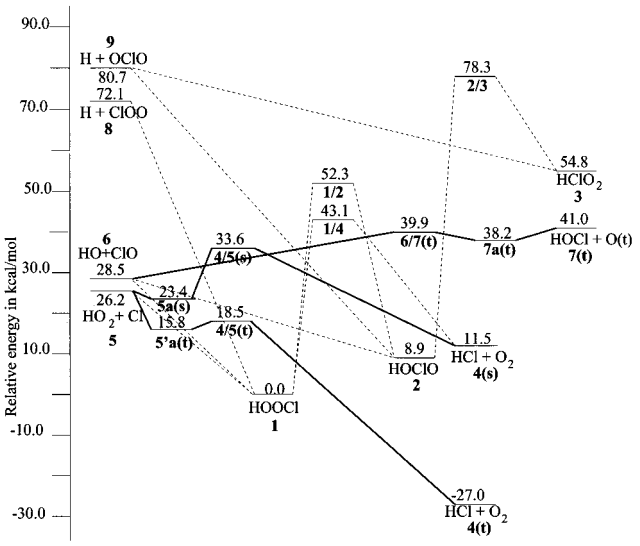

Figure 1. Overall profile of the potential energy surface for the [$HClO_2$] system calculated at B3LYP/6-311++G(2df,2pd) level of-theory. Solid lines represent the bimolecular direct hydrogen abstraction channels.

Results and Discussion

The PES of the [$HClO_2$] system as obtained from the B3LYP/6-311++G(2df,2pd) level of calculation is shown in Figure 1. The energies in Figure 1 are shown relative to that of the HOOCl adduct with appropriate zero-point vibrational energy corrections. Each stationary point in this figure is labeled with a number in order to facilitate the discussion. While the minima are associated with numbers from **1** to **9**, the transition structures (TS) connecting two minima **X** and **Y** are defined by **TSX/Y**. Furthermore, some of the stationary points are suffixed with a (s) or (t) to indicate their occurrence in the singlet or the triplet PES.

The optimized geometry for the equilibrium conformation of the various isomers of [$HClO_2$] at different levels of calculation are tabulated in Table 1 while the absolute energies (in hartrees) and zero-point vibrational energies (ZPVE) (in kcal/mol) of all the species are tabulated in Table 2. The different first-order saddle points on [$HClO_2$] PES are shown in Figure 2. The optimized structures of the various hydrogen-bonded complexes are shown in Figure 3. The calculated unscaled harmonic vibrational frequencies of the isomers of [$HClO_2$] are tabulated in Table 3 while those of other stationary points on the PES are tabulated in Table 4.

Geometry and Stability of the Adducts. The ground-state configuration for the peroxy radical possessing a bent H−O_2

TABLE 1: Equilibrium Geometries for $HClO_2$ Isomers from Different Treatments and Comparison with Previous Work[a]

molecule	coordinate	B3LYP/ 6-311++G (2df,2pd)[b]	MP2(FU)/ 6-311++G (d,p)[b]	MP2/ 6-311G (2d,2p)[c]	MP2/ 6-311G (d,p)[c]	MP2/ 6-31G*[c]	CCSD(T)/ TZ2P[c]	CAS[b] (12,12)/ 6-31G**[b]
HOOCl	HO	0.970	0.968	0.965	0.966	0.980	0.968	0.950
	OO	1.409	1.416	1.423	1.408	1.437	1.443	1.448
	OCl	1.738	1.740	1.750	1.751	1.739	1.746	1.758
	HOO	102.5	101.4	100.7	101.3	100.6	100.6	100.6
	OOCl	110.2	109.2	108.1	109.2	108.1	108.6	108.0
	HOOCl	88.4	92.6	88.2	89.7	90.2	89.1	92.6
HOClO	HO	0.969	0.970	0.966	0.968	0.983	0.968	0.977
	OCl	1.719	1.776	1.752	1.774	1.754	1.755	1.768
	ClO	1.517	1.505	1.503	1.500	1.513	1.536	1.543
	HOCl	104.6	104.0	101.9	102.9	104.1	102.3	103.0
	OClO	112.1	114.8	114.6	115.3	115.6	112.5	115.5
	HOClO	79.7	74.9	78.7	74.3	75.7	79.1	79.2
$HClO_2$	HCl	1.363	1.347	1.336	1.344	1.353	1.351	1.319
	ClO	1.481	1.484	1.472	1.480	1.488	1.497	1.501
	HClO	101.5	101.3	100.9	101.3	101.5	101.4	101.7
	OClO	115.9	118.2	117.3	118.1	118.7	116.5	118.6
	HOClO	109.0	109.5					110.3

[a] Bond lengths are given in Å and bond angles in deg. [b] From the present work. MP2(Fu) refers to the approach in which correlation of all electrons including the core are considered. [c] From ref 19.

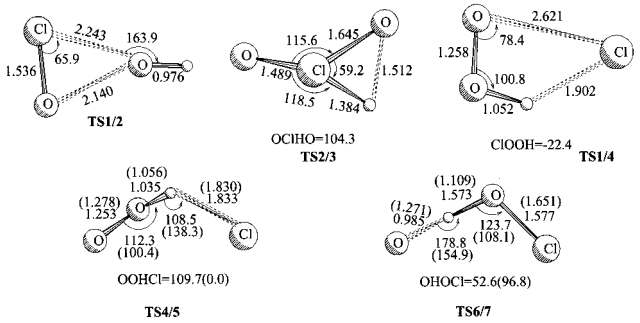

Figure 2. B3LYP/6-311++G(2df,2pd)-optimized structural parameters of the saddle points on the $[HClO_2]$ surface. Numbers in parentheses correspond to the geometry of the triplet state.

TABLE 2: Total Energies (E_T, in hartrees) and Zero-Point Energies (ZPE, in kcal/mol) for the Various Stationary Points on the $[HClO_2]$ Surface

molecule	E_T(ZPE)	molecule	E_T(ZPE)
HOOCl (**1**)	−611.180 199 (10.7)	HOClO (**2**)	−611.165 443 (10.4)
$HClO_2$ (**3**)	−611.091 250 (9.6)	**TS1/2**	−611.094 091 (8.9)
TS2/3	−611.050 120 (7.4)	**TS1/4**	−611.107 886 (8.4)
TS4/5(t)	−611.150 786 (7.2)	**TS4/5(s)**	−611.123 293 (8.6)
TS6/7(s)	−611.057 997 (7.4)	**TS6/7(t)**	−611.107 926 (5.3)
4a(s)	−611.157 849 (7.4)	**7a(t)**	−611.116 656 (9.0)
5a(s)	−611.141 433 (9.8)	**5′a(t)**	−611.154 136 (10.1)
$ClOO^{\bullet}$	−610.552 878 (2.9)	$OClO^{\bullet}$	−610.540 264 (3.5)
$ClO^{\bullet}$	−535.362 613 (1.2)	$HO^{\bullet}$	−75.765 572 (5.3)
HOCl	−536.020 121 (8.3)	HClO	−535.934 006 (6.1)
Cl_2O	−995.579 514 (2.3)	H_2O	−76.463 542 (13.4)
H_2O_2	−151.611 901 (16.7)	$HO_2^{\bullet}$	−150.967 189 (8.9)

nuclear framework is $1a'^2 2a'^2 3a'^2 4a'^2 5a'^2 1a''^2 6a'^2 7a'^2 2a''^1$. The attack of $Cl^{\bullet}$ at the terminal oxygen atom of $HO_2^{\bullet}$, where a major fraction of the radical electron density resides, leads to the stable covalently bonded HOOCl (**1**) intermediate. The geometry of the adduct was computed without any symmetry constraint. The equilibrium conformation of this molecule has not been determined experimentally. However, from the present computations as well as those of earlier works,[18,19] the minimum-energy structure is found to be skewed. In the following discussion, we consider the results obtained at CCSD(T)/TZ2P level to be more accurate while estimating the performance of the B3LYP level. The HOOCl dihedral angle at the B3LYP level of computation is predicted to be 88.4. Our optimized parameters of (**1**) using B3LYP and CAS(12,12) levels are tabulated in Table 1 and are compared with the corresponding data of earlier work employing MP2 and CCSD(T) approaches.

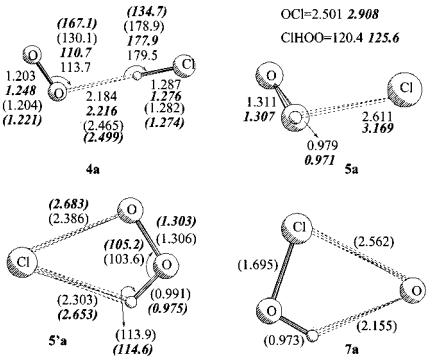

Figure 3. B3LYP/6-311++G(2df,2pd)-optimized geometries of the loose complexes on the $[HClO_2]$ surface. Numbers in parentheses correpond to the geometry of the triplet state. Numbers in italics were obtained at MP2(fu)/6-311++G** level of optimization.

TABLE 3: Comparison of the Harmonic Vibrational Frequencies of $HClO_2$ Isomers As Obtained from MP2/ 6-31G*, MP2(FU)/6-311++G, CCSD(T)/TZ2P, and B3LYP/6-311++G(2df,2pd) Levels**

molecule	approx vibrational description	MP2/ 6-31G*[a]	MP2(FU)/ 6-311++G**[b]	CCSD(T)/ TZ2P[a]	B3LYP[b]
HOOCl	HO stretch	3669	3785	3744	3707
	HOO bend	1418	1396	1399	1416
	OO stretch	870	874	835	898
	ClOO bend	685	657	633	636
	torsion	395	386	392	430
	ClO stretch	379	379	361	374
HOClO	HO stretch	3654	3776	3755	3737
	HOCl bend	1206	1141	1186	1188
	ClO stretch	1172	1071	935	972
	OCl stretch	584	503	540	614
	torsion	422	395	393	408
	OClO bend	302	289	249	323
$HClO_2$	HCl stretch	2243	2370	2168	2172
	ClO_2 sym stretch	1100	1074	1022	1033
	HClO sym bend	1065	1031	905	949
	OClO bend	424	421	415	434
	ClO_2 asym stretch	1227	1171	1093	1117
	HClO asym bend	1101	1065	1009	1031

[a] From ref 19. [b] From the present work.

TABLE 4: Unscaled B3LYP/6-311++G(2df,2pd) Harmonic Vibrational Frequencies of the Various Stationary Points on the PES of the [$HClO_2$] System

species	frequencies (cm^{-1})	ZPE (kcal/mol)
TS1/2	481i, 326, 385, 899, 954, 3666	8.9
TS2/3	1545i, 345, 708, 807, 1026, 2283	7.4
TS1/4	600i, 251, 551, 1268, 1419, 2385	8.4
TS6/7(t)	1469i, 135, 450, 788, 1016, 1292	5.3
TS6/7(s)	1412i, 72, 271, 629, 878, 3350	7.4
TS5/4(t)	618i, 194, 821, 981, 1295, 2107	7.7
TS5/4(s)	546i, 234, 419, 1281, 1372, 2680	8.6
4a(s)	51, 108, 233, 330, 1627, 2858	7.4
4a(t)	28, 56, 160, 171, 1639, 2940	7.1
5a(s)	124, 214, 340, 1147, 1429, 3569	9.8
5′a(t)	193, 258, 628, 1203, 1429, 3352	10.1
7a(t)	125, 173, 300, 734, 1298, 3666	9.0

It is worth mentioning that the geometries obtained at CAS(12,12)/6-31G** and CCSD(T)/TZ2P levels are in excellent agreement with each other except for a difference of 3° in the dihedral angle. The calculated OO bond length shows large variations with the level of treatment and it varies by ~0.02 and ~0.03 Å, respectively, at the MP2 and B3LYP levels. Of the MP2 calculations with various basis sets, the one with the 6-311G(2d,2p) basis set has led to a similar result as CAS(12,12)/6-31G** level signifying the importance of polarization functions over the diffuse functions. Geometries corresponding to both the planar cis and trans orientation were identified as transition structures. At the B3LYP level, the magnitude of the trans and cis barriers are respectively 4.0 and 6.0 kcal/mol. The CAS(12,12) calculations have shown that the contribution (squared weight $|c_i^2|$) of the ground-state configuration to the total wave function expansion amounts to 0.91; the contribution of the configuration arising from the two-electron excitation from HOMO to LUMO is 0.02.

In addition to the HOOCl arrangement there are two further isomers: (2) HOClO and (3) $HClO_2$ as a result of the hypervalent chlorine atom. In HOClO, the OCl and ClO bonds have different bond lengths. The values computed for OCl vary considerably with the method employed (Table 1). The MP2 calculations tend to give larger values than CCSD(T) while the DFT/B3LYP calculations underestimate this bond length by 0.036 Å relative to the CCSD(T) value. For the ClO bond the MP2 and DFT calculations both give lower values than the CCSD(T); this, in turn, means that the difference between OCl and ClO bonds is represented quite satisfactorily by the DFT approach (0.2 Å) relative to the more elaborate CCSD(T) calculation which predicts 0.22 Å for this difference. In order to test whether the ground state of HOClO can be basically represented by a single configuration, CAS(12,12) computations have also been undertaken. The dominant configuration shows a weight of 0.89 (measured by the square of the expansion coefficient) in the CAS expansion and confirms the single-configuration nature of the HOClO ground state. Both OCl and ClO bond lengths are larger in this CAS treatment, but this is presumably due to the smaller AO basis set; the difference between the two bond length is again calculated to be 0.22 Å.

The third isomeric form corresponds to a pentavalent chlorine. This structure possesses C_{2v} symmetry. The ClO bond in (**3**) is somewhat shorter (0.036 Å by B3LYP, 0.039 by CCSD(T)) than the terminal Cl═O distance in (**2**) due to resonance effects. The calculated value for the HCl bond obtained from DFT/B3LYP and the MP2 approaches is pretty much in line with those from the CCSD(T) treatment. On the other hand, there is a 0.03 Å difference in the HCl bond length as predicted by the CAS(12,12) and CCSD(T) calculation. Since the ground-state configuration has a contribution of 0.91 (measured by the square of the expansion coefficient) to the lowest-energy CAS(12,12) wave function, the ground state of $HClO_2$ (**3**) can also be considered a single-configuration state. Hence the difference in HCl bond length obtained from CCSD(T) and CAS(12,12) is probably due to the smaller AO basis set size in the CAS calculation. It is not surprising that polarization functions are most important for isomers **2** and **3** as they are associated with the valence expansion of the chlorine center.

At B3LYP level, the relative stability of the three isomers is of the order (**1** < **2** < **3**) (Table 2). HOOCl is 8.9 and 54.8 kcal/mol (Figure 1) lower in energy than HOClO and $HClO_2$, respectively. The harmonic vibrational frequencies of the [$HClO_2$] isomers are tabulated in Table 3. The B3LYP-predicted frequencies are in reasonable agreement with the prior CCSD(T) values. The largest difference of 74 cm^{-1} occurs for OCl stretch and OClO bending frequencies in HOClO. The heat of formation for the three isomers were calculated using the isodesmic reactions

$$HOCl + HOOH \rightarrow HOOCl + H_2O + \Delta E_1 \qquad (a)$$

$$Cl_2O + 2HOOH \rightarrow 2HOOCl + H_2O + \Delta E_2 \qquad (b)$$

as suggested in ref 18. The experimental heat of formation of HOCl, HOOH, H_2O, and Cl_2O are taken from the same reference. The magnitude of ΔE_1 and ΔE_2 at the B3LYP level is −8.2 and −13.6 kcal/mol, respectively. Combining these with the experimental ΔH_f^0 values, we obtain ΔH_f^0(HOOCl) = 0.8 and 0.6 kcal/mol from reactions a and b. Lee and Rendell[16] using CCSD(T)/TZ2P calculations found $\Delta H_{f,0}^0$ (HOOCl) to be 1.5 kcal mol^{-1}. We note that the B3LYP approach underestimates the heat of formation of HOOCl relative to the CCSD(T) value by 0.7 kcal/mol. However, it is interesting that Francisco et al.[19] have also found a heat of formation value for HOOCl very similar to our B3LYP value in their MP4/6-311++G(3df,3pd) calculations. HOOCl is bound, respectively, by 28.5, 26.2, and 72.1 kcal/mol with respect to the dissociation limits HO + ClO, HO_2 + Cl and H + ClOO. Lee and Rendell[18] estimated these dissociation energies by using the experimental $\Delta H_f^{298.5}$ quantities and arrived at values of 33.4, 31.4, and 73.4 kcal/mol for the corresponding dissociation limits. In spite of minor quantitative disagreements, the performance of DFT calculations with the B3LYP functional in predicting the equilibrium structures, vibrational frequencies, and relative energies for the three isomers is reasonably good in comparison to the corresponding values from the CCSD(T) calculations and moreover the pertinent values are obtained with a remarkably less amount of computational costs.

Isomerization of $HClO_2$ Isomers. The 1,2-migration of the OH group from the oxygen to the chlorine atom results in the HOClO isomer. The minimum-energy path of HOOCl → HOClO isomerization has been traced and the optimal geometry of the transition state **TS1/2** is located. Structural analysis of the three-membered transition state, **TS1/2**, reveals an elongated O···O and O···Cl bonds while the analysis of the eigenvectors corresponding to the negative eigenvalue of the force constant matrix suggests the reaction vector to be composed of OClO bending. The reaction vector corresponding to the imaginary frequency (480.8i) is

$$-0.24r_{OO} - 0.67\theta_{HOCl} + 0.68\theta_{OClO}$$

The vibration which has lost during the course of this reaction is ClOO bending. This isomerization, however, involves a high barrier (52.3 kcal/mol) and **TS1/2** is disposed energetically

TABLE 5: Results of B3LYP/6-311++G(2df,2pd) Calculations for the Intrinsic Reaction Coordinate of $HO_2 + Cl \rightarrow HCl + {}^3O_2$

energy (kcal/mol)	react coord	$R_{H\cdot\cdot O}$ (Å)	R_{OO} (Å)	$R_{Cl\cdots H}$ (Å)	∠HOO (deg)	∠ClHO (deg)
−611.216 34	−2.498	2.044	1.204	1.285	123.0	176.5
−611.215 49	−2.298	1.940	1.204	1.288	121.5	175.3
−611.214 13	−2.098	1.836	1.204	1.291	120.1	174.1
−611.212 06	−1.898	1.732	1.204	1.298	118.9	172.7
−611.209 01	−1.698	1.628	1.205	1.309	117.8	171.0
−611.204 60	−1.498	1.528	1.205	1.334	116.7	169.1
−611.198 40	−1.299	1.435	1.207	1.380	115.8	166.9
−611.190 33	−1.099	1.354	1.209	1.444	114.9	164.6
−611.181 05	−0.899	1.284	1.213	1.518	113.9	161.9
−611.171 65	−0.699	1.221	1.219	1.597	112.6	158.6
−611.162 94	−0.499	1.166	1.229	1.674	110.3	154.4
−611.155 59	−0.299	1.118	1.245	1.744	106.6	148.9
−611.151 27	−0.099	1.076	1.266	1.801	102.2	142.1
−611.150 79	0.000	1.057	1.277	1.830	100.4	138.3
−611.151 07	0.099	1.041	1.287	1.863	99.2	134.5
−611.151 63	0.198	1.029	1.294	1.904	99.0	131.3
−611.152 24	0.298	1.020	1.298	1.949	99.3	128.6
−611.152 79	0.398	1.013	1.300	1.996	99.9	126.1
−611.153 25	0.498	1.006	1.302	2.044	100.5	124.0
−611.153 60	0.598	1.002	1.303	2.093	101.1	121.9
−611.153 86	0.698	0.998	1.304	2.142	101.7	120.0
−611.154 03	0.798	0.995	1.304	2.192	102.3	118.1
−611.154 13	0.897	0.993	1.305	2.241	102.9	116.2
−611.154 17	0.997	0.991	1.305	2.290	103.5	114.5

above the reactants, OH + ClO, as well as the dissociation limit, HO_2 + Cl. Hence, in the reaction kinetics of OH + ClO, this isomerization is not expected to play any significant role at ordinary temperatures. However, it will have a contribution toward the total rate constant, if the entrance channel happens to be H + ClOO•.

The third isomer, $HClO_2$, can be obtained from HOClO via a 1,2-hydrogen shift and the transition state for such a process **TS2/3** is shown in Figure 2. The migrating hydrogen is respectively 1.38 and 1.51 Å away from the migrating terminus and the origin. This isomerization is highly endothermic (45.9 kcal/mol) and involves a very high barrier (69.4 kcal/mol) and lies above the HO• + ClO•, HO_2• + Cl, and H + ClOO• dissociation limits. Hence, formation of $HClO_2$ (**3**) is highly improbable in the reactions of OH + ClO and HO_2 + Cl•. Structurally, **TS2/3** is close to the product **3** in accord with the Hammond's postulate. Nonetheless, the existence of the reverse barrier (23.5 kcal/mol) and the barrier for its dissociation into H• + OClO• (25.9 kcal/mol) in the PES reveal the high stability of this hypervalent chlorine compound.

Mechanism of HCl + $^{1,3}O_2$ Formation. Metathesis reaction of HO_2 radical, HO_2 + Cl → HCl + O_2, can proceed either via a direct abstraction of hydrogen or a complex mechanism involving a four-membered transition state from the stable HOOCl adduct. In the former, a bimolecular abstraction of the hydrogen by attack on the σ_{OH} bond of HO_2• leads to hydrogen chloride and oxygen molecule while the latter involves a 1,2-elimination of HCl from HOOCl and it proceeds via **TS1/4**. The product HCl + $^1O_2$ is 14.7 kcal/mol lower in energy than the reactants, HO_2 + Cl, and the barrier for its formation via HOOCl is high, ∼43.1 kcal/mol above the stabilized HOOCl intermediate. For the corresponding process, Weissman et al.,[15] estimated an unusually low barrier height (25.7 ± 3 kcal/mol). The barrier height obtained in this work is in comparison with those of the analogous reaction[15] from chlorinated ethanes (38−56 kcal/mol). The facts that **TS1/4** is located above the dissociation products, OH + ClO, and that the Arrhenius preexponential factor for dissociation is generally large in magnitude as it involves a very loose transition state relative to that of the tight transition state, **TS1/4** unquestionably rule out the possibility of HCl + O_2 formation from the adduct.

Direct hydrogen abstraction by the doublet chlorine radical from HO_2 radical can occur from either of the singlet and triplet surfaces. The dominant interaction between the two species is the attack of the singly occupied orbital of chlorine on the doubly occupied σ_{OH} orbital of HO_2. The bonding and antibonding orbitals are created respectively by the positive and negative overlap of the same two orbitals of the reactant. The antibonding orbital has significant O_2 character. This suggests that the transition state of higher multiplicity (with triplet oxygen character) should be the more stable of the two possible spin states. In addition, on the triplet surface the reaction leads to the formation of the more stable triplet oxygen molecule. The saddle points corresponding to the abstraction of hydrogen from the singlet and triplet surfaces have been located, and the optimized structures are shown in Figure 2. The numbers within parantheses correspond to the triplet state. The reaction is exothermic by 53.2 and 14.7 kcal/mol, respectively, on the triplet and singlet surfaces. The energy of the triplet transition state **TS4/5(t)** lies below that of HO_2 + Cl reactants. We identified a loose hydrogen-bonded complex between HO_2 and Cl on the triplet, **5a′ (t)** surface.

The pathway for the hydrogen abstraction is summarized in Table 5. These data were obtained by following the IRC calculation from **TS4/5(t)** back to the reactant and forward to the products. The data presented here were determined at B3LYP/6-311++G(2df,2pd) level to present a more accurate picture of the geometric changes. As shown in Table 5, the dominant change as the molecule proceeds to the product are represented by an elongation of the H−O bond in conjunction with a shortening of the H−Cl bond length. The O−O bond length decreases due to the formation of a π bond along this pathway. Also the angle made by the abstracting chlorine atom with oxygen widens up along the path. Minima were found on both sides of the reaction coordinate and are shown in Figure 3. The geometry of this minimum was optimized further at MP2 level to check for the artifacts of the B3LYP method and the optimized geometry at the MP2 level are shown in Figure 3 in bold italics font. Hence, on the triplet surface, the weak hydrogen-bonded complex formed by the electronegative chlorine has sufficient excess energy to cross over saddle point, **TS4/5(t)**. This thereby suggests that the reaction proceeds without

any appreciable barrier and explains the unusually large magnitude of the rate constant. The magnitude of the imaginary frequency is 617.5i cm^{-1}. The reaction vector is the asymmetric ClHO stretch ($-0.32r_{HO} + 0.63r_{HCl} + 0.67\theta_{ClHO}$) and the ClHO bending vibration. The hydrogen abstraction is angular and the ClHO angle is 138.3°.

The optimized geometrical parameters of the **TS4/5(s)** have similar magnitude as in **TS4/5(t)** except for the O−O distance and OOHCl dihedral angle. The **TS4/5(s)** lies 9.5 kcal/mol below the saddle point for the four-centered elimination, **TS1/4**. This undoubtedly eliminates the involvement of the four-center elimination mechanism in HCl formation. Therefore, the singlet oxygen formation, if it occurs, will proceed preferably via direct hydrogen abstraction.

In addition to the hydrogen-bonded complex, **5′a(t)**, yet another complex (**5a(s)**) wherein chlorine interacts with the OH group of HO_2 radical has been located on the singlet surface. This singlet biradical complex [Cl···HO_2] **5a(s)** lies energetically ∼2.1 kcal/mol below the HO_2 + Cl limit. This is in accord with Weismann's[15] supposition that the incoming chlorine faces a greater attractive interactionat the oxygen end of the HO_2 radical (∼26.2) on the singlet surface instead of the hydrogen end. Hence, on the singlet surface the reaction leads to HOOCl adduct as it is a barrierless recombination. Since subsequent isomerizations and dissociations involve appreciable barriers, it would redissociate back to the reactants. Nevertheless, the kinetics of HO_2 + Cl reaction will be dominated by the triplet oxygen formation via direct hydrogen abstraction.

Mechanism of HOCl + ^{1,3}O Formation. In the reactions of HO + ClO, besides the formation of the stable covalently bound HOOCl adduct, the reaction could also proceed via the abstraction of hydrogen by the $ClO^{\bullet}$ radical leading to atomic oxygen product. This reaction can take place on either the singlet or the triplet electronic surface. On the singlet surface, since the formation of the adduct is a barrierless process, it will supersede the abstraction channel. However, on the triplet surface, direct abstraction could be the major channel. The reaction is endothermic by 12.5 kcal/mol and is found to have a barrier of 11.4 kcal/mol. A loose van der Waals complex between triplet oxygen and HOCl (**7a(t)**) has been identified and it has all real frequencies (Table 4). Hence, when the reactants have energy equal to or greater than that of **TS6/7(t)**, this channel will contribute in the rate expression. The direct hydrogen abstraction transition structure on the singlet surface involves very high barrier and is shown in Figure 2 for the sake of completion.

Kinetics of HO + ClO and HO_2 + Cl Reaction: a Qualitative Overview. The competitive pathways for the disappearance of the reactants in the HO + ClO reaction are

$$HO + ClO \underset{}{\overset{k_1}{\rightleftharpoons}} HOOCl \xrightarrow{k_2} HO_2 + Cl$$

$$HO + ClO \rightleftharpoons HOClO$$

$$HO + ClO \rightarrow HOCl + {}^3O$$

The hydroxyl radical can attack at either the oxygen or the chlorine end of the ClO radical. Formation of both isomers, **1** and **2**, is a barrierless process and is accessible for the thermal HO + ClO reactants. The only pathway that is available to the energized **2*** at ordinary temperatures and pressures is redissociation. The energized HOOCl, however, has sufficient energy for either a redissociation back to the reactants or to a dissociation into HO_2 and Cl radicals. Of these two possibilities, the latter predominates owing to its low barrier height and it thereby explains the experimental observation of the branching ratio, k_{1a}/k_1. As can be seen from Figure 1, the energy needed for O−O dissociation in HOOCl is 2.3 kcal/mol more than that for O−Cl dissociation. Hence, in order for HOOCl to be isolated from HO + ClO, the energy-rich complex must be deactivated below the limit for decomposition into HO_2 and Cl. Importantly, the present PES portrays 100% of chain transfer process. Most of the HO_2 thus derived is expected to have excess internal energy. The temperature dependence of this reaction is dictated by the magnitude as well as the dependence of k_{-1} and k_2 with temperature. We expect the direct hydrogen abstraction pathway to play a certain role at higher temperatures. On the other hand, the reaction kinetics of HO_2 + Cl reaction

$$HO_2 + Cl \xrightarrow{\text{TS4/5(t)}} HCl + {}^3O_2 \qquad \text{(Path A)}$$

$$HO_2 + Cl \rightleftharpoons HOOCl \rightarrow HO + ClO \qquad \text{(Path B)}$$

$$HO_2 + Cl \xrightarrow{\text{TS4/5(s)}} HCl + {}^1O_2 \qquad \text{(Path C)}$$

is determined predominantly by the abstraction channel path A leading to the highly exothermic HCl + $^3O_2$ product in addition to the adduct **1** formation. The formation of the weak hydrogen-bonded intermediate **5′a(t)** explains the large magnitude of the rate constant and accounts for the negative temperature dependence of the rate constant. Since energetically accessible dissociation routes are not available for the covalently bound **1**, redissociation to HO_2 and Cl will be the favored channel from HOOCl*. At high temperatures, O−O dissociation is expected to compete with the O−Cl dissociation. Singlet oxygen formation will occur preferably via direct hydrogen abstraction.

If isomers of $HClO_2$ were to be isolated in the HO + ClO, HO_2 + Cl, and/or H + $ClOO^{\bullet}$ recombination reactions, then the excess energy (above the HO_2 + Cl limit) available to the isomers must be removed by a spontaneous energy transfer with the collision partner in the reaction medium.

Conclusions

The present study provides the first consistent and fairly complete study of the transition-state geometries and barrier heights for the isomerization, molecular elimination, and direct hydrogen abstraction channels on the [$HClO_2$] PES. Furthermore, an attempt has been made to demonstrate the applicability of density functional approach to treat the hypervalent isomers of [$HClO_2$]. In addition, the present PES qualitatively explains the observed reaction kinetics. Though for many years four-center elimination has been the favored mechanism for HCl and O_2 formation, this study, beyond any doubt, reveals that attack at the hydrogen atom is the most promising pathway for the disappearance of HO_2 and Cl reactants. Since O−Cl bond dissociation energy is lower than the barrier height at **TS1/4**, dissociation from the initially formed HOOCl* is more favorable than isomerization or a four-centered elimination of HCl, in the reactions of hydroxyl radical with ClO. Atomic oxygen formation is expected to contribute at higher temperatures.

Acknowledgment. R.S. thanks the Alexander von Humboldt Stiftung for financial support.

References and Notes

(1) Sumathi, R.; Peyerimhoff, S. D. *J. Chem. Phys.* **1997**, *107*, 1872.
(2) Nguyen, M. T.; Sumathi, R.; Sengupta, D.; Peeters, J. *Chem. Phys.* **1998**, *230*, 1.
(3) Leu, M. T.; Lin, L. L. *Geophys. Res. Lett.* **1979**, *6*, 425.

(4) Ravishankara, A. R.; Eisele, F. L.; Wine, P. H. *J. Chem. Phys.* **1983**, *78*, 1140.
(5) Hills, A. J.; Howard, C. J. *J. Chem. Phys.* **1984**, *81*, 4458.
(6) Burrows, J. P.; Wallington, T. J.; Wayne, R. P. *J. Chem. Soc., Faraday Trans. 2* **1984**, *80*, 957.
(7) Poulet, G.; Laverdet, G.; Le Bras, G. *J. Phys. Chem.* **1986**, *90*, 159.
(8) Leu, M.-T.; DeMore, W. B. *Chem. Phys. Lett.* **1976**, *41*, 121.
(9) Poulet, G.; Le Bras, G.; Combourieu, J. *J. Chem. Phys.* **1978**, *69*, 767.
(10) Burrows, J. P.; Cliff, D. I.; Harris, G. W.; Thrush, B. A.; Wilkinson, J. P. T. *Proc. R. Soc. London Ser. A* **1979**, *368*, 463.
(11) Baulch, D. L.; Cox, R. A.; Hampson, Jr., R. F.; Kerr, J. A.; Troe, J., Watson, R. T. *J. Phys. Chem. Ref. Data* **1980**, *9*, 295.
(12) Cox, R. A. *Int. J. Chem. Kinet.* **1980**, *12*, 649.
(13) Cox, R. A., Derwent, R. G. *J. Chem. Soc., Faraday Trans. 1* **1977**, *73*, 272.
(14) Lee, Y−P.; Howard, C. J. *J. Chem. Phys.* **1982**, *77*, 756.
(15) Weissman, M.; Shum, L. G. S.; Heneghan, S. P.; Benson, S. W. *J. Phys. Chem.* **1981**, *85*, 2863.
(16) Mozurkewich, M. *J. Phys. Chem.* **1986**, *90*, 2216.
(17) Toohey, D. W.; Anderson, J. G. *J. Phys. Chem.* **1989**, *93*, 1049.
(18) Lee, T. J.; Rendell, A. P. *J. Phys. Chem.* **1993**, *97*, 6999.
(19) Francisco, J. S.; Sander, S. P.; Lee, T. J.; Rendell, A. P. *J. Phys. Chem.* **1994**, *98*, 5644.
(20) Fan, L.; Ziegler, T. *J. Chem. Phys.* **1990**, *92*, 3645. Stanton, R. V.; Merz, K. M., Jr. *J. Chem. Phys.* **1994**, *100*, 434. Baker, J.; Andzelm, J.; Muir, M.; Taylor, P. R. *Chem. Phys. Lett.* **1995**, *237*, 53. Baker, J.; Muir, M.; Andzelm, J. *J. Chem. Phys.* **1995**, *102*, 2063. Nguyen, M. T.; Creve, S.; Vanquickenborne, L. G. *J. Phys. Chem.* **1996**, *100*, 18422. Margl, P.; Ziegler, T.; Blöchl, P. E. *J. Am. Chem. Soc.* **1995**, *117*, 12625. Torrent, M.; Deng, L.; Duran, M.; Sola, M.; Ziegler, T. *Organometallics* **1997**, *16*, 13. Deng, Q.; Thomas, B. E., IV; Houk, J. N.; Dowd, P. *J. Am. Chem. Soc.* **1997**, *119*, 6902.
(21) Jursic, B. S. *Chem. Phys. Lett*. **1999**, *299*, 334.
(22) Frisch, M. J.; Trucks, G. W.; Gordon, M. H.; Gill, P. M. W.; Wong, M. W.; Foresman, J. B.; Johnson, B. G.; Schlegel, H. B.; Robb, M. A.; Replogle, E. S.; Gomperts, R.; Andres, J. L.; Raghavachari, K.; Binkley, J. S.; Gonzalez, C.; Martin, R. J.; Fox, D. J.; Defrees, B. J.; Baker, J.; Stewart, J. J. P.; Pople, J. A. *Gaussian 94*; Gaussian Inc.: Pittsburgh, PA, 1994.
(23) Becke, A. D. *J. Chem. Phys.* **1993**, *98*, 5648.
(24) Lee, C.; Yang, W.; Parr, R. G. *Phys. Rev. B* **1986**, *33*, 8822.
(25) Gonzales, C.; Schlegel, H. B. *J. Chem. Phys.* **1989**, *90*, 2154. Gonzales, C.; Schlegel, H. B. *J. Phys. Chem.* **1990**, *94*, 5523. Deng, L.; Ziegler, T. *Int. J. Quantum Chem.* **1994**, *52*, 731.
(26) Werner, H.-J.; Knowles, P. J. (with contributions from: Almlof, J.; Amos, R. D.; Deegan, M. J. O.; Elbert, S. T.; Hampel, C.; Meyer, W.; Peterson, K.; Pitzer, R.; Stone, A. J.; Taylor, P. R.) MOLPRO version 94.10, 1994.